THE JOURNAL OF PHYSICAL CHEMISTRY LETTERS
A JOURNAL OF THE AMERICAN CHEMICAL SOCIETY

pubs.acs.org/JPCL

Letter

Ultrafast Collective Excited-State Dynamics of a Virus-Supported Fluorophore Antenna

Joseph Holmes,[§] Arathi Anil Sushma,[§] Irina B. Tsvetkova,* William L. Schaich, Richard D. Schaller, and Bogdan Dragnea*

Cite This: *J. Phys. Chem. Lett.* 2022, 13, 3237−3243

Read Online

ACCESS | Metrics & More | Article Recommendations | Supporting Information

ABSTRACT: Radiation brightening was recently observed in a multifluorophore-conjugated brome mosaic virus (BMV) particle at room temperature under pulsed excitation. On the basis of its nonlinear dependence on the number of chromophores, the origins of the phenomenon were attributed to a collective relaxation. However, the mechanism remains unknown. We present ultrafast transient absorption and fluorescence spectroscopic studies which shed new light on the collective nature of the relaxation dynamics in such radiation-brightened, multifluorophore particles. Our findings indicate that the emission dynamics is consistent with a superradiance mechanism. The ratio between the rates of competing radiative and nonradiative relaxation pathways depends on the number of chromophores per virus. The findings suggest that small icosahedral virus shells provide a unique biological scaffold for developing nonclassical, deep subwavelength light sources and may open new avenues for the development of photonic probes for medical imaging applications.

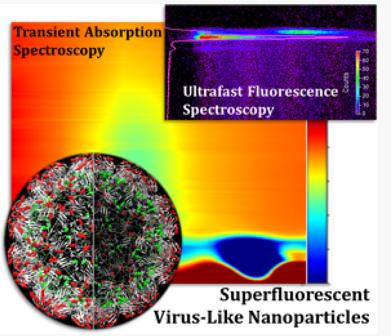

High-contrast luminescent nanoprobes enable myriad applications, including biological detection,[1] therapeutics,[2,3] sensing,[4,5] optogenetics,[6,7] and anticounterfeiting.[8,9] For the vast majority of current probes, radiation is the result of random, spontaneous relaxation. Consequently, emission dynamics obeys classical exponential decay.[10] Because background emission has similar dynamics, time-domain background removal to improve contrast is seldom a viable option in imaging applications. Increasing the number of emitters per nanoprobe to augment brightness generally results in self-quenching due to interemitter distances becoming short enough ($\lesssim$5 nm) for efficient resonant energy transfer to occur. Both challenges could be addressed by constructing a multiemitter nanoprobe with correlated, nonclassical emission. In this Letter we present experimental evidence for this behavior, which is found to occur when a dense array of hundreds of fluorescent dyes, deterministically arranged on a 28 nm diameter icosahedral virus template, is excited by an ultrafast laser pulse.

Radiation brightening from dye-conjugated fluorescent virus-like particles (fVLPs) was first reported by Tsvetkova et al.[11] It was found that when the chromophores are conjugated to the reactive residues of the brome mosaic virus (BMV) at capsid interfaces, emission by the complex is strongly accelerated with respect to that of the free dye.[11] The brightening effect was found to be a nonlinear function of $\langle N \rangle$, the average number of chromophores per particle. Specifically, as $\langle N \rangle$ increased, an initial quenching of the fluorescence was observed. When $\langle N \rangle$ exceeded ∼150 chromophores/particle, the quenching was suppressed and fluorescence was restored. Because of limited time resolution and other detector limitations, the dynamics of restored fluorescence emission remained unknown, but it was clear that it was significantly shorter than that of free chromophores. Thus, the origins of the phenomenon were attributed to a collective effect.[11,12] To obtain additional information about the mechanism of radiation brightening in fVLPs, we performed measurements of the emission and the excited-state relaxation dynamics.

We found that instead of the several nanosecond exponential decay expected from individual chromophores in solution, emission from a multifluorophore virus particle, at saturation coverage, occurs as a short burst of ∼20 ps. Peak intensity is attained at ∼25 ps after the ultrafast excitation pulse. Instead of being nearly quenched like under continuous-wave excitation, the estimated quantum yield in burst-mode is comparable to that of free, individual chromophores. These unusual characteristics occur at room temperature, in a biocompatible setting. Such viromimetic probes are promising to overcome some of the current limitations of classical biophotonic probes and open new venues in fluorescence imaging.

In this work, a fluorescein-derived dye, Oregon Green 488, was covalently bound to the BMV capsid via NHS ester

Received: January 26, 2022
Accepted: March 28, 2022
Published: April 5, 2022

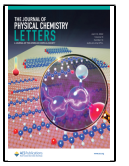

https://doi.org/10.1021/acs.jpclett.2c00262
J. Phys. Chem. Lett. 2022, 13, 3237−3243

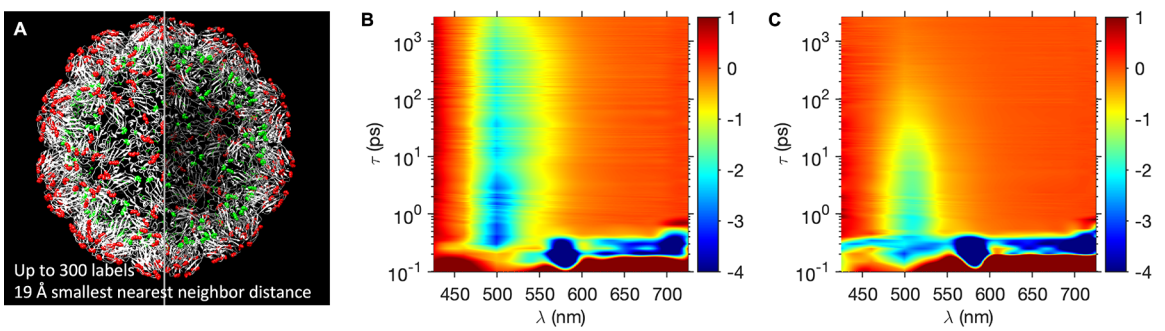

Figure 1. (A) Schematic of accessible labeling sites on BMV capsid: red, external lysines K64, K105, and K165; green, internal lysines K41, K44, and K86. (B and C) Transient absorption surface plots of free OG and BMV-OG278 following an initial excitation at 7.1 mJ/cm^2. The color scale corresponds to the difference between the absorbance of the samples in excited and ground states (units of mΔA).

labeling of exposed lysines.[11] The maximum labeling density was ∼300 dyes/virus[11] (see Figure S1). Figure 1A shows a molecular model of BMV, with the dye-accessible external and internal lysines colored in red and green, respectively.[12] Here "internal" means located between the lumenal and outer capsid surfaces. The minimum nearest neighbor distance between lysines was estimated to be 1.9 nm.[11] Because of negligible nearest-neighbor electronic coupling (Figure S1), no spectral changes were observed in the absorption or emission spectra as a function of N.

To follow the excited-state dynamics of coupled chromophores in fVLPs as compared with free chromophores in solution, we performed pump−probe femtosecond, transient absorption (TA) spectroscopy. Differential absorption (ΔA) spectra of isolated chromophores and fVLP samples with an average number of 278 dyes per particle (termed BMV-OG278) are presented as a function of the wavelength and time-delay in panels B and C of Figure 1, respectively. The ultrafast excitation pulse at 488 nm was provided by an optical parametric amplifier pumped by a regenerative amplifier (∼120 fs pulse width). The particular choice of wavelengths has been made to operate the pump as close as possible to the maximum absorption of virus-bound chromophores because it was shown before that a high number of excited chromophores is necessary for collective emission.[11]

In both the free dye control and the BMV-OG278 sample, two intense negative signals are evident at very early times in the transient spectra (Figure 1). One appears at 570−580 nm, and it can be attributed to Raman scattering of water.[13] Because this event is simultaneous with the excitation pulse, its appearance defines the zero delay between pump and probe pulses. The second, early negative signal is due to the coherent interaction between pump and probe pulses, which leads to stimulated Raman amplification appearing at 650−750 nm.[14] Both Raman signals vanish within 0.4 ps from the pump pulse.

A spectral region of particular interest is 500−540 nm, where ground-state bleach (GSB) is expected. Indeed, both sample and control exhibit a prominent feature in this spectral region (Figure 1B,C). However, there are also some stark differences between the two: In particular, the excited-state decay is much faster for the BMV-OG278 sample than for the free dye solution.

The minima in ΔA spectra at 498 nm for free dye and 504 nm for VLP-bound chromophores are consistent with the peak wavelengths for steady-state absorption (Figure S1), which supports their assignment as GSB features. The 5−6 nm shift between free and bound chromophores is attributable to the difference in the dielectric constant between protein and water. The stimulated emission induced by the probe laser is expected to overlap with fluorescence emission wavelengths (peak emission at 510−515 nm for free dye and at 518−525 nm for bound chromophores), be more prominent at higher pump fluences, and show a shift in the SE peak position with time. No such characteristics have been observed in the evolution-associated decay spectra (Figures S3−S7) or in the global fitting results (see below).

Global analysis was performed on the raw TA data sets to obtain decay-associated spectra (DAS) for free and VLP-bound dyes (Figures S8−S12). For the free dye, global analysis yielded single DAS with characteristic times longer than 2 ns, which we associate with GSB. In contrast, BMV-OG produced two DAS: one with characteristic times of $\gtrsim$1 ns and one with ∼25 ps. The long characteristic time DAS is similar to the free chromophore DAS. Note that the short characteristic time DAS has a prominent extremum at $\lambda \approx 510$ nm, red-shifted from peak absorption wavelength for the free dye (498 nm) and from the bound chromophores (504 nm), suggesting the fast relaxation pathway occurs in a subset of chromophores in agreement with previous findings.[12]

To gain access to the weights of each contribution to the kinetic traces, TA spectra were integrated from 520 to 530 nm and fitted with an exponential model from 400 fs to 2.6 ns (Figures S14−S18). For analysis, the wavelength and time-delay range were chosen past the ground-state bleach minimum to avoid artifacts from pump laser scattering and to remove coherent artifacts which arise around the zero delay time where the pump and probe beams are temporally overlapping.[15,16] Exponential fit parameters (amplitude and decay time) were obtained by means of the nonlinear least-squares method, and the estimates of the errors from the model were computed from the sample covariance matrix. Best fit kinetic models for the transients were found to be predominantly monoexponential for the free fluorophore and biexponential for the virus-bound fluorophore. Normalized amplitudes (A_i) and decay times (τ_i) obtained from the fit procedure are presented as a function of $\langle N \rangle$ in the plots in Figure 2, with $\langle N \rangle = 0$ corresponding to free chromophores in solution.

At low pump fluence, the excited-state lifetime (τ_1) of free dyes measured by TA was on average ∼3.3 ns, which matches the spontaneous emission lifetime of OG in solution. Because the quantum yield is high for this dye, fluorescence emission is the dominant pathway in the relaxation dynamics of the free fluorophore excited at 488 nm. The long lifetime component

https://doi.org/10.1021/acs.jpclett.2c00262
J. Phys. Chem. Lett. 2022, 13, 3237−3243

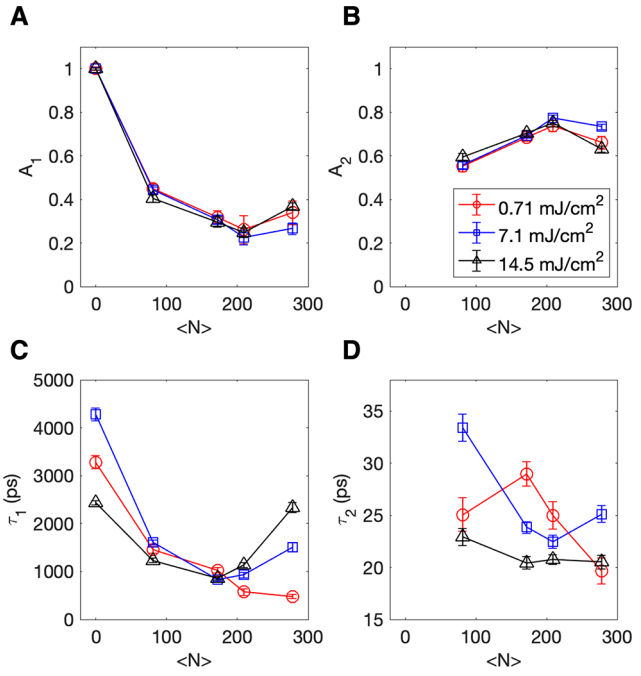

Figure 2. Fit components for the excited-state decay dynamics plotted against varying $\langle N \rangle$, i.e., number of chromophores/virus. Top panels: amplitudes A_1 and A_2. Bottom panels: Lifetimes (τ_1) and (τ_2).

(τ_1) exhibits a monotonic shortening as the number of bound dyes increases (Figure 2C, red curve). At high labeling density, the τ_1 is reduced by a factor of 6 when compared to the free fluorophore. This shortening of the lifetime matches that of previous fluorescence lifetime experiments at similar excitation fluences and $\langle N \rangle$ where the fluorescence lifetime was shortened, and the photon counts were quenched upon an initial increase in $\langle N \rangle$.[11] This is because at low pump fluence, the number of simultaneous excitations per pulse is small. The majority of chromophores are in the ground state, and there is a high probability for homo-resonance energy transfer (RET) to occur, with the indirect result of commonly observed concentration quenching.[17,18] Thus, we note a correlation between the evolution of the TA τ_1 and that of the streak camera measured fluorescence decay.

As the pump fluence increases, τ_1 decreases for the free dye, possibly due to an increase in intersystem crossing and triplet-state formation[19] or, in a lesser extent, to photobleaching. Indeed, typically, 10−20% photobleaching was observed between the first and second run for each sample. However, at high labeling density ($\langle N \rangle \gtrsim 200$), τ_1 increases from ∼600 ps at lowest pump fluence up to ∼2000 ps for highest pump fluence. Thus, it appears that the nonradiative rate, which was deemed responsible for the initial shortening of the lifetime at low fluences and high density,[11] slows down to a value that is observed only at lower labeling densities. This suggests that a subset of chromophores relax as they were isolated from the others.

The second fit component (parameters A_2 and τ_2) dominates BMV-OG dynamics at short times. Therefore, a new relaxation channel has opened that operates only in high-load multifluorophore VLPs. The associated amplitude A_2 is significantly greater than A_1 (Figure 2B). Its time constant is $\tau_2 \approx 25-35$ ps for low and medium fluence and ∼20−25 ps for the highest pump fluence (Figure 2D). This component appears to decrease with the number of dyes per virus, although the trends are noisy (Figure 2D).

To summarize up to this point, two factors appear to lead to changes in the excited-state dynamics: (i) pump fluence at fixed $\langle N \rangle$ and (ii) $\langle N \rangle$ at all fluences. Specifically, relaxation dynamics is accelerated when $\langle N \rangle$ increases.

While fluorophore coupling clearly affects relaxation lifetimes, the result of the competition between nonradiative and radiative relaxation channels cannot be gauged based on solely TA. To obtain further spectral and temporal information on fluorescence emission, we have performed time-resolved fluorescence spectroscopy with a streak-camera detector. Panels A and B of Figure 3 present spectrally and time-resolved fluorescence emission for free fluorophore and BMV-OG204, respectively. The pump pulse arrives at $t_0 \approx 110$ ps. Raman scattering from water, at ∼560−580 nm, is simultaneous with the pump pulse. Also, a faint spot at t_0 can be observed at ∼500−510 nm in free OG and BMV-OG samples. This is due to elastic scattering of the laser line being incompletely suppressed by laser rejection filters. The scattering peak is very faint in the case of free OG because this sample does not scatter as strongly as the virus particles. The inelastic and the elastic scattering peaks are convenient because they facilitate the timing of fluorescence emission with respect to the pump pulse.

For free dye samples, emission is spread in time and decays uniformly along the entire measured time interval (Figure 3 A,C). In stark contrast, the fluorescence from the BMV-OG

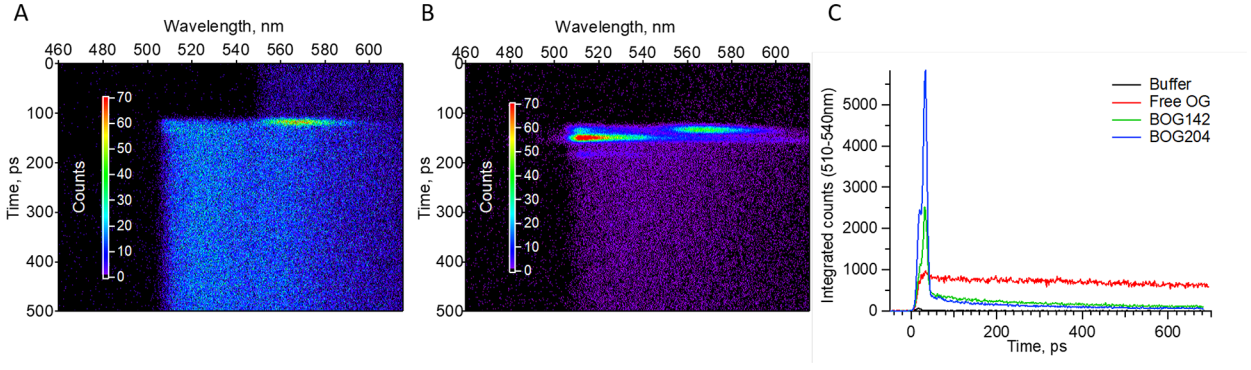

Figure 3. Dynamics of fluorescence emission using a streak-camera detector. The total dye concentration for all samples was kept at 200 nM, and the laser energy density was 16.2 mJ/cm^2. (A) Free OG dye. (B) BMV-OG204. (C) Wavelength-integrated (510−540 nm), time-resolved fluorescence decay traces for BMV-OG and controls.

https://doi.org/10.1021/acs.jpclett.2c00262
J. Phys. Chem. Lett. 2022, 13, 3237−3243

samples is emitted as a burst of ~20 ps duration. The burst is delayed with respect to the pump pulse, with a maximum occurring at $t \approx 25$ ps after excitation (Figure 3B,C). At this point, we note that the value of τ_2 from TA measurements is close to the characteristic time of the fluorescence burst observed in the streak-camera experiment. This observation is consistent with the short relaxation pathway observed in TA corresponding to radiative relaxation. The wavelength-integrated peak amplitude of the burst shows a 2× increase when $\langle N \rangle$ is increased from ~140 to ~200 dyes per virus (Figure 3C).

What phenomena could potentially be responsible for the delayed, nonexponential, accelerated radiation in VLPs? We consider superfluorescence (SF), superradiance (SR), and amplified spontaneous emission (ASE).[20,21] Although we are not completely excluding the possibility of lasing, i.e., light amplification by stimulated emission, we note that it is less likely, at least in the conventional sense, because of the absence of a resonator, the extremely small VLP volume, and thus the small Purcell factor.[22]

There are qualitative differences between ASE and SF in both the time and frequency domains. In the frequency domain, SF(SR) emission occurs in a broader window,[23] while in ASE, spectral narrowing is expected as pump intensity increases.[24] Both steady-state and pulsed emission spectra were studied previously, and no spectral narrowing could be observed.[11] However, ASE cannot be ruled out based on solely the absence of observable line narrowing argument because of the relative low maximum fluence at which our experiments were performed. Nevertheless, a few other characteristics are useful in discriminating between ASE and SF, as discussed in the following.

In the time domain, the SF pulse is sharp and develops after a time delay.[25] The fluorescence emission dynamics presented in Figure 3 clearly shows a 25 ps delay with respect to the arrival of the excitation pulse. In ASE, the time delay is vanishingly small, the output pulse is generally longer than in SF and noisy, and the pulse duration is insensitive to dephasing factors (e.g., local viscosity and temperature).[26−28] In this context, as shown in previous work[11,12] the radiation brightening from multifluorophore VLPs is very sensitive to the local environment. Indeed, the introduction of a longer linker between the virus template and the chromophore or substitution of the viral template by a silica nanobead completely suppressed the collective emission.[11] This would be hard to explain within the ASE framework, which is much less sensitive to dephasing, but it would be reasonably expected if we were dealing with SR or SF. Second, solutions are extremely dilute. ASE involving multiple particles will not happen at such concentrations. On the other hand, ASE within individual VLPs is unlikely because the total number of emitters is too small.

A rough estimate of the number of coupled chromophores can be made by using the cooperative lifetime (τ_r) formula:[28]

$$\tau_r = \frac{8\pi \mathcal{A}}{3\lambda^2} \cdot \frac{T_1}{N} \tag{1}$$

where $\mathcal{A}$ is the area of the VLP; T_1 is the reciprocal of the Einstein coefficient A; and N is the number of coupled chromophores, which in general is expected to be smaller than the average number of supported chromophores $\langle N \rangle$. For a $\tau_r \approx 15$ ps, one estimates a number $N \approx 30$ (see also the simple no-dephasing two-level model in the Supporting Information, section "A simple model of superradiant emission dynamics", and Figure S19 for an illustration of the emission dynamics.) This value, which is smaller than the $\langle N \rangle$ value at the threshold, supports the previous findings that a subset of chromophores is responsible for the effect.[12]

A striking similarity exists between the time evolution in Figure 3C and the theoretical plot of the temporal evolution of the N atom cooperative spontaneous emission in ref 28 (Figure 4a,b in ref 28). Note that even the small temporal ringing was reproducibly observed in the fVLP streak camera experiments (see Figure 3B−C at $t \approx 60$ ps after excitation).

Therefore, the delayed, intense pulse of the fluorescence emission prominently exhibiting a nonclassical time-dependence in streak camera experiments, the broad fluorescence spectrum, and the sensitivity to the fluorophore local environment all point to a superradiance-like mechanism responsible for radiation brightening. Moreover, a striking feature is the fact that the phenomenon occurs at room temperature, in solution. By contrast, SR emission dynamics was extensively experimentally studied in atomic gases at very low temperatures.[29] Later, it was also detected in solids,[30−34] and molecular aggregates, at cryogenic temperatures.[35,36]

Only recently SR was shown to occur at room temperature in photosynthetic complexes.[37,38] The structured environment within the photosynthetic complex is believed to promote collective fluorophore behavior because rigidity and proper orientation can alleviate thermal dephasing.[39] In support of this idea, alterations in the relative position and orientation of chromophores in the protein pockets of an artificial photosynthetic system were found to strongly affect the excited-state dynamics of protein-bound chromophores.[40,41] However, it is worth emphasizing that interfluorophore interactions in light-harvesting complexes and in most molecular J-aggregates are characterized by strong coupling.[42−44]

By comparison, the nearest-neighbor fluorophore distances on BMV-OG are much longer than that of molecular aggregates, which precludes electron tunnelling and points to a qualitatively different mechanism. In our case, collective emission of radiation arises from weak coupling at room temperature. Until now, this coupling range has not been given much attention. Dipole−dipole coupling is considered detrimental to the formation of coherent multifluorophore states.[29] The "decohering" effect of dipole−dipole coupling should be suppressed when the coupling interaction is symmetrical by atom exchange. Could the virus template symmetry play a role in enforcing this condition? The original model of Dicke superradiance (see the Supporting Information) and indeed, to the best of our knowledge, most theoretical approaches that followed do not take into account the spatial organization or orientation of the chromophores. However, from previous work[11,12] it is clear that the nature of the template is important for the radiation brightening effect. This interesting, open question warrants future studies of the system presented here.

The virus template provides a molecular architecture that is uniquely accurate relative to other nanotemplates. However, the nature of chemical conjugation implies heterogeneity at several levels. Specifically, we know that there are three broadly defined chemical environments for the fluorophores.[12] These three environments have distinct labeling kinetics,[11] which means that one first saturates a domain (obtaining a reasonably homogeneous sample) before the second, and so on. The first to get labeled is the internal (lumenal) interfacial environment,

https://doi.org/10.1021/acs.jpclett.2c00262
J. Phys. Chem. Lett. 2022, 13, 3237−3243

where fluorophores bind to unstructured, flexible N-termini. We know that removing the lumenal sites does not suppress the radiation brightening effect. Thus, it is unlikely that the lumenal fluorophore subset is responsible for the collective behavior. This does not imply that it should be ignored in future models; because of short interfluorophore distances, RET is likely to occur between the correlated subset, after the superradiant burst, and the still-excited fluorophores of the uncorrelated lumenal interface subset. The second subset is at the outer surface. Preliminary experiments could not detect collective behavior in the emission from surface-labeled residues.[12] We note that orientational freedom is expected to be increased at the outer surface. The third subset is buried within the structural part of the capsid. These sites get labeled at high pH, when the virus shell is swollen. Optical measurements are done at low pH, where the shell is in a compressed state and has a well-defined, symmetric structure. This subset, characterized by low orientational freedom, is currently the most likely candidate responsible for the bulk of the collective response. Whole virus, all-atom molecular dynamics studies are underway to quantify the differences in these three environments in terms of orientational fluctuations.

Note that labeling site heterogeneity will occur even at saturation labeling. Another type of inherent heterogeneity, which could limit SF, is related to the (unknown) size of the coherent domain: how many fluorophores can emit collectively, even in a homogeneous subset labeled at saturation, at room temperature? Time-dependent fluctuations are expected to limit the correlation length. The latter can be estimated by second-order photon correlation measurements, which are underway in our laboratory.

Finally, the chemical conjugation approach will result in kinetic labeling coverage fluctuations, especially in conditions below saturation. Single-particle FLIM experiments (see scatter plot in Figure 3 of ref 11) have indeed shown that, below the loading threshold at which SF is observed, the variance in particle intensity is the largest at low $\langle N \rangle$. This suggests that particle loading heterogeneity decreases as one approaches labeling saturation. However, when the loading threshold for SF is reached, the variance (and the mean) for single-particle intensity increase significantly. A possible explanation is that the SF is sensitive to a different set of conditions, as discussed above, than uncorrelated emission.

In conclusion, the symmetric, 28 nm diameter of the BMV capsid provides a biological scaffold for a multifluorophore array that acts as an antenna with accelerated emission rate at room temperature that concentrates, at each pulse, ∼200 eV of light energy in a subwavelength volume, yielding an estimated power density of approximately 1 TW/cm^3. It is conceivable that such power densities could be harnessed in the future to perform efficient localized photochemical transformations. To unveil the mechanistic characteristics of the phenomenon we have employed time-resolved fluorescence dynamics approaches coupled with ultrafast transient absorption. Upon excitation near saturation by pulsed irradiation, neighboring chromophores are excited simultaneously and lateral resonant-energy transfer and concentration quenching are largely suppressed. At the same time, the excited virus-supported chromophores couple directly by dipole−dipole interactions or possibly via the template and relax cooperatively as the strong dependence of the relaxation and the characteristic emission times on the number of chromophores suggest.

Enhanced light intensity, nonclassical emission dynamics, and biocompatibility make viromimetic superfluorescent particles promising for biological imaging at high background conditions, as deep tissue optical probes, and as nano-light sources for localized photochemical transformations.

EXPERIMENTAL SECTION

BMV-OG Sample Preparation. BMV-OG samples were prepared according to protocols previously described.[11] Briefly, the lysines of wtBMV were modified by covalent conjugation with Oregon Green 488 carboxylic acid, succinimidyl ester.[45] wtBMV stock in SAMA buffer (50 mM NaOAc, 8 mM $Mg(OAc)_2$ (pH 4.6)) was mixed with sodium bicarbonate buffer (100 mM, pH 8.2) in 1:1 ratio to a final concentration of 10^{13} particles/ml. Dye stock was freshly prepared in DMSO and was added to virus solution at varied ratios ranging from 500 to 10000 dyes/capsid. The DMSO concentration in reaction mixture was kept constant at ∼5 w/v%. The reaction was left for 1−2 h at room temperature, followed by removal of free dye via filter wash or dialysis with SAMA buffer. UV−vis spectroscopy was performed to estimate the number of dyes per virus, and fluorescence spectroscopy was used to confirm the absence of free dyes in the purified samples.

Transmission Electron Microscopy. Electron-transparent samples were prepared by placing the dilute sample (10 μL) onto a carbon-coated copper grid. After 10 min, excess solution on the grid was removed with filter paper. The grid was stained with uranyl acetate (10 μL of 2% solution) for 10 min, and the excess solution was removed by blotting with filter paper. The sample was then left to dry for several minutes. Images were acquired at an accelerating voltage of 80 kV on a JEOL JEM 1010 transmission electron microscope and analyzed with the ImageJ Processing Toolkit (see the Supporting Information).

Time-Resolved Pulsed Excitation Fluorescence Spectroscopy with Streak Camera. The sample was excited by a pulse generated through an optical parametric amplifier using a Ti:sapphire femtosecond laser (Spectra-Physics Spitfire Pro). The pulses have a wavelength of λ = 480 nm, a duration of 35 fs, and a repetition rate of 2000 Hz. The focused spot size was measured to be 160 μm, and the average laser power varied from 1 to 6.5 mW (or 0.5 to 3.25 μJ/pulse). The excitation beam was directed at the cuvette at a small angle to prevent cavity effect. The sample fluorescence was collected with a lens, directed through a long pass filter (LP508) and a 150 mm spectrograph, and then was detected as a function of wavelength and time after excitation using a photon counting streak camera (Hamamatsu C5680). Data were collected and preprocessed by HPDTA software, and further analysis was done with Igor Pro software.

Transient Absorption Spectroscopy. Ultrafast transient absorption measurements were carried out using an output of a regeneratively amplified Ti:sapphire laser (800 nm, 120 fs, 2 kHz repetition rate) which was split into two beams. The first beam, containing 10% power, was focused into a sapphire crystal to generate a white light continuum (440−750 nm), which serves as the probe laser. The other beam, containing 90% of the power, was sent into an optical parametric amplifier to generate the 480 nm pump beam. After passing through a depolarizer, the pump beam is focused and overlapped with the probe beam at the sample (focal diameter being 300 μm). The sample was placed in 2 mm quartz cuvette equipped with stirring bar to reduce sample photobleaching. For each sample, two scans were acquired, compared, and found to exhibit

https://doi.org/10.1021/acs.jpclett.2c00262
J. Phys. Chem. Lett. 2022, 13, 3237−3243

negligible differences. These scans were averaged and used for data analysis. The pump pulse fluence was varied from 0.71 to 14.2 mJ/cm^2, while the probe pulse fluence was significantly smaller and kept constant in all experiments. Because of uncertainty of estimation of focal spot and absorption cross section of chromophore antenna, the pump fluences were chosen to be well below, close to, and well above the estimated saturation point for photon density per virus (see Table 1).

Table 1. Photometric Quantities for $\langle N \rangle$ = 300

average laser power (mW)	fluence (mJ/cm^2)	absorbed photons/pulse/virus
1	0.71	30
10	7.1	300
20	14.2	600

The number of absorbed photons per pulse per particle was estimated by using single-molecule absorption cross section calculated from molar absorption coefficient, $\sigma = 0.56 \times 10^{-16}$ cm^2. Prior to any analysis, spectra were corrected for chirp and group dispersion velocity using Surface Explorer (Ultrafast Systems).

■ ASSOCIATED CONTENT

Supporting Information

The Supporting Information is available free of charge at https://pubs.acs.org/doi/10.1021/acs.jpclett.2c00262.

Experimental methods, sample characterization, TA fitting results, and model of superradiant emission from N chromophores (PDF)

Transparent Peer Review report available (PDF)

■ AUTHOR INFORMATION

Corresponding Authors

Irina B. Tsvetkova − *Department of Chemistry, Indiana University, Bloomington, Indiana 47405, United States*; Email: itsvetko@indiana.edu

Bogdan Dragnea − *Department of Chemistry, Indiana University, Bloomington, Indiana 47405, United States*; orcid.org/0000-0003-0611-2006; Email: dragnea@indiana.edu

Authors

Joseph Holmes − *Physics Department, Indiana University, Bloomington, Indiana 47405, United States*

Arathi Anil Sushma − *Department of Chemistry, Indiana University, Bloomington, Indiana 47405, United States*

William L. Schaich − *Physics Department, Indiana University, Bloomington, Indiana 47405, United States*

Richard D. Schaller − *The Center for Nanoscale Materials at Argonne National Laboratory, Lemont, Illinois 60439, United States*; orcid.org/0000-0001-9696-8830

Complete contact information is available at: https://pubs.acs.org/10.1021/acs.jpclett.2c00262

Author Contributions

§J.H. and A.A.S. contributed equally to this work.

Notes

The authors declare no competing financial interest.

■ ACKNOWLEDGMENTS

The work was supported by the Army Research Office, under Awards W911NF2010072 and W911NF2010071, and by the National Science Foundation, under Award CBET-1803440. This work was performed, in part, at the Center for Nanoscale Materials, a U.S. Department of Energy Office of Science User Facility, and supported by the U.S. Department of Energy, Office of Science, under Contract No. DE-AC02-06CH11357. We are grateful to the Center for Bioanalytical Metrology (CBM), an NSF Industry-University Cooperative Research Center, for providing funding for this project under Grant NSF IIP 1916645, and to members of the industry advisory board of the CBM for valuable discussions and feedback.

■ REFERENCES

(1) Wolfbeis, O. S. An overview of nanoparticles commonly used in fluorescent bioimaging. *Chem. Soc. Rev.* **2015**, *44*, 4743−4768.

(2) Yi, X.; Wang, F.; Qin, W.; Yang, X.; Yuan, J. Near-infrared fluorescent probes in cancer imaging and therapy: an emerging field. *Int. J. Nanomed.* **2014**, *9*, 1347.

(3) Vats, M.; Mishra, S. K.; Baghini, M. S.; Chauhan, D. S.; Srivastava, R.; De, A. Near infrared fluorescence imaging in nano-therapeutics and photo-thermal evaluation. *International journal of molecular sciences* **2017**, *18*, 924.

(4) Ueno, T.; Nagano, T. Fluorescent probes for sensing and imaging. *Nat. Methods* **2011**, *8*, 642−645.

(5) Gao, L.; Wang, W.; Wang, X.; Yang, F.; Xie, L.; Shen, J.; Brimble, M. A.; Xiao, Q.; Yao, S. Q. Fluorescent probes for bioimaging of potential biomarkers in Parkinson's disease. *Chem. Soc. Rev.* **2021**, *50*, 1219−1250.

(6) Leopold, A. V.; Shcherbakova, D. M.; Verkhusha, V. V. Fluorescent biosensors for neurotransmission and neuromodulation: engineering and applications. *Frontiers in cellular neuroscience* **2019**, *13*, 474.

(7) Oheim, M.; van't Hoff, M.; Feltz, A.; Zamaleeva, A.; Mallet, J.-M.; Collot, M. New red-fluorescent calcium indicators for optogenetics, photoactivation and multi-color imaging. *Biochimica et Biophysica Acta (BBA)-Molecular Cell Research* **2014**, *1843*, 2284−2306.

(8) Abdollahi, A.; Roghani-Mamaqani, H.; Razavi, B.; Salami-Kalajahi, M. Photoluminescent and chromic nanomaterials for anticounterfeiting technologies: recent advances and future challenges. *ACS Nano* **2020**, *14*, 14417−14492.

(9) Li, M.; Feng, Y.; Tian, Q.; Yao, W.; Liu, L.; Li, X.; Wang, H.; Wu, W. Tunable and ultra-stable UV light-switchable fluorescent composites for information hiding and storage. *Dalton Transactions* **2018**, *47*, 11264−11271.

(10) Valeur, B.; Berberan-Santos, M. r. N. *Molecular fluorescence: principles and applications*, 2nd ed.; John Wiley & Sons: New York, 2013.

(11) Tsvetkova, I. B.; Anil Sushma, A.; Wang, J. C.-Y.; Schaich, W. L.; Dragnea, B. Radiation brightening from virus-like particles. *ACS Nano* **2019**, *13*, 11401−11408.

(12) Anil Sushma, A.; Zhao, B.; Tsvetkova, I. B.; Pérez-Segura, C.; Hadden-Perilla, J. A.; Reilly, J. P.; Dragnea, B. Subset of fluorophores is responsible for radiation brightening in viromimetic particles. *J. Phys. Chem. B* **2021**, *125*, 10494−10505.

(13) Parker, C. Raman spectra in spectrofluorimetry. *Analyst* **1959**, *84*, 446−453.

(14) Lorenc, M.; Ziolek, M.; Naskrecki, R.; Karolczak, J.; Kubicki, J.; Maciejewski, A. Artifacts in femtosecond transient absorption spectroscopy. *Appl. Phys. B: Laser Opt.* **2002**, *74*, 19−27.

(15) Vardeny, Z.; Tauc, J. Picosecond coherence coupling in the pump and probe technique. *Opt. Commun.* **1981**, *39*, 396−400.

(16) Liu, H.; Zhang, H.; Si, J.-H.; Yan, L.-H.; Chen, F.; Hou, X. Elimination of the coherent artifact in a pump-probe experiment by

directly detecting the background-free diffraction signal. *Chin. Phys. Lett.* **2011**, *28*, 086602.
(17) Beddard, G. S.; Porter, G. Concentration quenching in chlorophyll. *Nature* **1976**, *260*, 366−367.
(18) Robeson, J. L.; Tilton, R. D. Effect of concentration quenching on fluorescence recovery after photobleaching measurements. *Biophys. J.* **1995**, *68*, 2145−2155.
(19) Demchenko, A. P. Photobleaching of organic fluorophores: quantitative characterization, mechanisms, protection. *Methods and Applications in Fluorescence* **2020**, *8*, 022001.
(20) Cong, K.; Zhang, Q.; Wang, Y.; Noe, G. T.; Belyanin, A.; Kono, J. Dicke superradiance in solids [invited]. *J. Opt. Soc. Am. B* **2016**, *33*, C80−C101.
(21) Dai, D. C. Brief comment: Dicke superradiance and superfluorescence find application for remote sensing in air. *arXiv* **2011**, 1108.5360.
(22) Samuel, I. D. W.; Namdas, E. B.; Turnbull, G. A. How to recognize lasing. *Nat. Photonics* **2009**, *3*, 546−549.
(23) Dicke, R. H. Coherence in spontaneous radiation processes. *Phys. Rev.* **1954**, *93*, 99−110.
(24) Allen, L.; Peters, G. Amplified spontaneous emission and external signal amplification in an inverted medium. *Phys. Rev. A* **1973**, *8*, 2031.
(25) Malcuit, M. S.; Maki, J. J.; Simkin, D. J.; Boyd, R. W. Transition from superfluorescence to amplified spontaneous emission. *Phys. Rev. Lett.* **1987**, *59*, 1189−1192.
(26) Wilk, S. R.; Boyd, R. W.; Teegarden, K. J. Laser characteristics of KCL: O-2. *Optics communications* **1983**, *47*, 404−406.
(27) Rai, J.; Bowden, C. M. Quantum-statistical analysis of superfluorescence and amplified spontaneous emission in dense media. *Phys. Rev. A* **1992**, *46*, 1522.
(28) Maki, J. J.; Malcuit, M. S.; Raymer, M. G.; Boyd, R. W.; Drummond, P. D. Influence of collisional dephasing processes on superfluorescence. *Phys. Rev. A* **1989**, *40*, 5135.
(29) Gross, M.; Haroche, S. Superradiance: an essay on the theory of collective spontaneous emission. *Phys. Rep.* **1982**, *93*, 301−396.
(30) Miyajima, K.; Kumagai, Y.; Ishikawa, A. Ultrashort radiation of biexcitonic superfluorescence from high-density assembly of semiconductor quantum dots. *J. Phys. Chem. C* **2017**, *121*, 27751−27757.
(31) Tighineanu, P.; Daveau, R. S.; Lehmann, T. B.; Beere, H. E.; Ritchie, D. A.; Lodahl, P.; Stobbe, S. Single-photon superradiance from a quantum dot. *Physical review letters* **2016**, *116*, 163604.
(32) Rainò, G.; Becker, M. A.; Bodnarchuk, M. I.; Mahrt, R. F.; Kovalenko, M. V.; Stöferle, T. Superfluorescence from lead halide perovskite quantum dot superlattices. *Nature* **2018**, *563*, 671−675.
(33) Krieg, F.; Sercel, P. C.; Burian, M.; Andrusiv, H.; Bodnarchuk, M. I.; Stöferle, T.; Mahrt, R. F.; Naumenko, D.; Amenitsch, H.; Rainò, G.; et al. Monodisperse long-chain sulfobetaine-capped CsPbBr3 nanocrystals and their superfluorescent assemblies. *ACS central science* **2021**, *7*, 135−144.
(34) Haider, G.; Sampathkumar, K.; Verhagen, T.; Nádvorník, L.; Sonia, F. J.; Valeš, V.; Sỳkora, J.; Kapusta, P.; Němec, P.; Hof, M.; et al. Superradiant emission from coherent excitons in van Der Waals heterostructures. *Adv. Funct. Mater.* **2021**, *31*, 2102196.
(35) Palacios, M. A.; de Weerd, F. L.; Ihalainen, J. A.; van Grondelle, R.; van Amerongen, H. Superradiance and exciton (de)localization in light-harvesting complex II from green plants? *J. Phys. Chem. B* **2002**, *106*, 5782−5787.
(36) Engel, G. S.; Calhoun, T. R.; Read, E. L.; Ahn, T.-K.; Mančal, T.; Cheng, Y.-C.; Blankenship, R. E.; Fleming, G. R. Evidence for wavelike energy transfer through quantum coherence in photosynthetic systems. *Nature* **2007**, *446*, 782−786.
(37) Monshouwer, R.; Abrahamsson, M.; van Mourik, F.; van Grondelle, R. Superradiance and exciton delocalization in bacterial photosynthetic light-harvesting systems. *J. Phys. Chem. B* **1997**, *101*, 7241−7248.
(38) Malina, T.; Koehorst, R.; Bína, D.; Pšenčík, J.; van Amerongen, H. Superradiance of bacteriochlorophyll c aggregates in chlorosomes of green photosynthetic bacteria. *Sci. Rep.* **2021**, *11*, 8354.
(39) Rolczynski, B. S.; Zheng, H.; Singh, V. P.; Navotnaya, P.; Ginzburg, A. R.; Caram, J. R.; Ashraf, K.; Gardiner, A. T.; Yeh, S.-H.; Kais, S.; et al. Correlated protein environments drive quantum coherence lifetimes in photosynthetic pigment-protein complexes. *Chem.* **2018**, *4*, 138−149.
(40) Noriega, R.; Finley, D. T.; Haberstroh, J.; Geissler, P. L.; Francis, M. B.; Ginsberg, N. S. Manipulating excited-state dynamics of individual light-harvesting chromophores through restricted motions in a hydrated nanoscale protein cavity. *J. Phys. Chem. B* **2015**, *119*, 6963−6973.
(41) Delor, M.; Dai, J.; Roberts, T. D.; Rogers, J. R.; Hamed, S. M.; Neaton, J. B.; Geissler, P. L.; Francis, M. B.; Ginsberg, N. S. Exploiting chromophore−protein interactions through linker engineering to tune photoinduced dynamics in a biomimetic light-harvesting platform. *J. Am. Chem. Soc.* **2018**, *140*, 6278−6287.
(42) Spano, F. C.; Mukamel, S. Superradiance in molecular aggregates. *J. Chem. Phys.* **1989**, *91*, 683−700.
(43) Meinardi, F.; Cerminara, M.; Sassella, A.; Bonifacio, R.; Tubino, R. Superradiance in molecular H aggregates. *Physical review letters* **2003**, *91*, 247401.
(44) Ratner, M. Superradiance of J-aggregates: correspondence between an infinite disordered chain and a regular finite chain. *Low Temperature Physics* **2003**, *29*, 602−605.
(45) Johnson, I., Spence, M., Eds. *The Molecular Probes Handbook: A Guide to Fluorescent Probes and Labeling Technologies*, 11th ed.; Life Technologies, 2010.

https://doi.org/10.1021/acs.jpclett.2c00262
J. Phys. Chem. Lett. 2022, 13, 3237−3243